

A self-complementary macrocycle by a dual interaction system

Received: 20 May 2022

Accepted: 14 September 2022

Published online: 26 September 2022

Check for updates

Yuta Sawanaka¹, Masahiro Yamashina¹✉, Hiroyoshi Ohtsu¹ & Shinji Toyota¹✉

Self-complementary assembly is one of the most promising phenomena for the formation of discrete assemblies, e.g., proteins and capsids. However, self-complementary assembly based on multiple host-guest systems has been scarcely reported due to the difficulty in controlling each assembly. Herein, we report a dual interaction system in which the key assembly direction is well regulated by both π - π stacking and hydrogen bonding to construct a self-complementary macrocycle. Continuous host-guest behavior of anthracene-based molecular tweezers during crystallization leads to successful construction of a cyclic hexamer, which is reminiscent of Kekulé's monkey model. Furthermore, the cyclic hexamer in a tight and triple-layered fashion shows hierarchical assembly into cuboctahedron and rhombohedral assemblies in the presence of trifluoroacetic acid. Our findings would be potentially one of metal-free strategies for constructing anthracene-based supramolecular assemblies with higher-order structure.

Ingenious molecules incorporating effective noncovalent bonding sites can form well-defined self-assemblies from a single class of molecules using their intrinsic properties. Such assemblies are often called “self-complementary assemblies”¹, which are frequently shown in nature². For example, the HIV-1 capsid is composed of the p24 protein hexamer, which is self-assembled by six protein subunits through multiple hydrogen bonds (Fig. 1a)^{3,4}. In supramolecular chemistry, abundant self-complementary assemblies have been reported on the basis of intrinsic hydrogen bonds^{5–8}, π -interactions^{9–12}, and coordination bonds^{13,14}. However, although host-guest behavior is a combination of multiple noncovalent interactions⁶ and ubiquitous phenomena in the field of science¹⁵, the construction of precise assemblies based on homologous host-guest systems is still a formidable challenge. This difficulty mainly arises for three reasons: (i) monomer design – both “host” and “guest” parts with high binding affinity have to be involved in a monomer molecule; (ii) binding mode – to progress consecutive bindings, the host-guest reactions should be carried out in an enclathration fashion, in which a host molecule partially binds to a guest¹⁶, rather than in a full encapsulation fashion; (iii) assembly direction – each host-guest complex should have sufficient rigidity since structural flexibility (i.e., less directionality of assembly)

leads to the formation of infinite assemblies. Due to these limitations, the number of discrete self-complementary assemblies realized by host-guest reactions is overwhelmingly low even in noncovalent bond¹⁷ and heterologous systems thus far¹⁸.

To demonstrate the construction of a discrete self-complementary assembly¹, we herein focused on a tweezer-like molecule (i.e., molecular tweezers), in which two aromatic panels are connected by a linker unit^{19,20}. Pyridinedicarboxamide (PDA) is often incorporated into various functional molecules since intramolecular hydrogen bonding regulates two substituents on N atoms into a *syn* form^{21,22}. According to recent achievements by Sessler's and Haino's research groups, PDA-based molecular tweezers can form self-complementary complexes in both head-to-head and head-to-tail modes^{23–25}. In particular, head-to-tail assembly tends to form linear supramolecular polymers through donor-acceptor promoted π - π interactions^{26,27}. We thus envisaged that providing a “regulated direction” to head-to-tail assembly as a secondary interaction could enable construction of a closed-ring assembly by capturing the other, such as the “six monkey model” of Kekulé's anecdote²⁸. To implement both donor-acceptor promoted π - π interactions and hydrogen bonding in concert, namely, the “dual interaction system”, we employed PDA-

¹Department of Chemistry, School of Science, Tokyo Institute of Technology, Tokyo, Japan. ✉e-mail: yamashina@chem.titech.ac.jp; stoyota@chem.titech.ac.jp

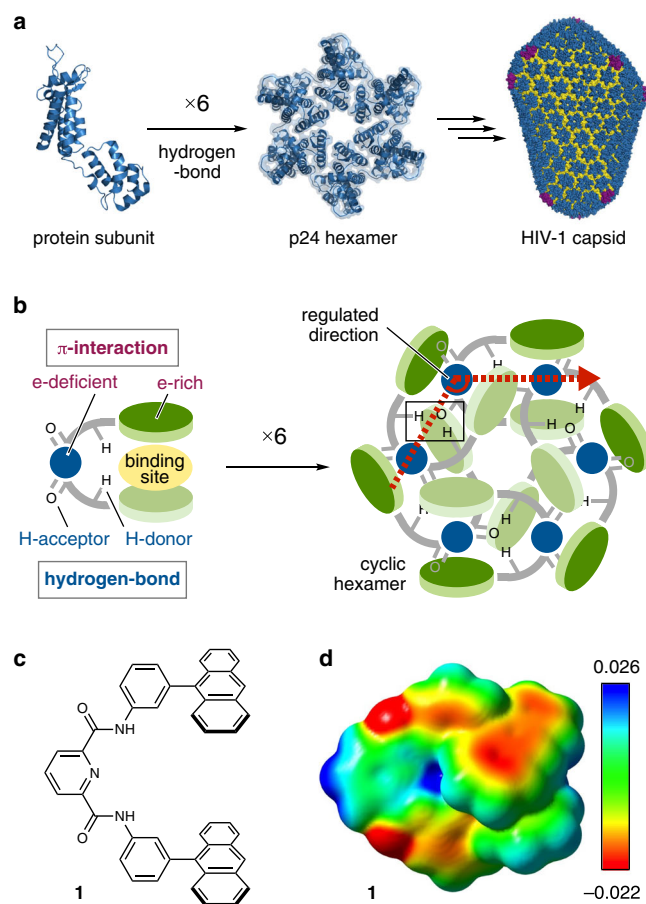


Fig. 1 | Schematic representations of self-complementary assembly. **a** Six protein subunits assembled through multiple hydrogen bonds to form a p24 protein hexamer of the HIV capsid. **b** Schematic representation of the dual interaction system for the construction of a self-complementary macrocycle in this work. **c** Chemical structure of anthracene-based molecular tweezers **1** and **d** its ESP map calculated by the density functional theory (DFT) method at the B3LYP-D3/6-31 G(d,p) level.

based molecular tweezers with polycyclic aromatic panels (Fig. 1b, left). Electron-rich aromatic units prefer to bind an electron-deficient pyridine ring moiety²⁹. Afterwards, the π - π interaction assists intermolecular hydrogen bonding between the inner NH (H-donor) and outer carbonyl (H-acceptor). As a consequence of dual interactions, the second tweezers would have an orientation with a regulated direction, leading to construction of a macrocycle via continuous host-guest behavior (Fig. 1b, right).

Here, we report anthracene-based molecular tweezers **1** with a PDA linker (Fig. 1c). The electron density of the anthracene panels is much higher than that of the pyridine moiety, as confirmed by the electrostatic potential (ESP) map (Fig. 1d). By employing the dual interaction strategy, a supramolecular macrocycle is exclusively and efficiently constructed in the solid state. X-ray and thermal analyses reveal that the macrocycle is sufficiently stable in the solid state. Moreover, a capsid-shaped very large assembly, in which 108 molecules are assembled into a cuboctahedron geometry, is obtained by further assembly of the macrocycles.

Results

Formation of a self-complementary dimer in a solution

Anthracene-based molecular tweezers **1** was synthesized by amidation of 2,6-pyridinedicarbonyl dichloride with 9-(3-aminophenyl)anthracene in 93% yield (Supplementary Figs. 1–6). In the concentration-

dependent ¹H NMR analysis in CDCl₃, pyridyl signals *H*_a and *H*_b showed a significant upfield shift upon increasing the concentration of **1**. These chemical shift changes arose from the aromatic shielding effect from the anthracene panels. Plotting the changes in chemical shift versus the concentration of **1** provided a binding curve that perfectly fits the simple dimerization model (Supplementary Fig. 17, Supplementary Table 1). The self-association constant *K*_a at 293 K was determined to be 314 M⁻¹. According to the van't Hoff plot, ΔH and $T\Delta S$ were estimated to be -27.3 kJ/mol and -13.3 kJ/mol, respectively. The formation of (**1**)₂ is thus an enthalpy-driven process. Interestingly, a theoretical study revealed that head-to-tail assembled dimer is more stable by 7.4 kJ/mol than head-to-head assembled dimer (Supplementary Fig. 18). The pyridine signals show the most intense upfield shift, indicating that tweezers **1** prefers to form head-to-tail dimer (**1**)₂ in CDCl₃.

Formation of a self-complementary macrocycle in the solid state

In contrast, tweezers **1** formed the head-to-tail hexamer in the solid state. The slow diffusion of *n*-hexane into a CH₂Cl₂ solution of **1** for 1 day afforded colorless crystals with the triclinic *P*-1 space group. Single-crystal X-ray analysis unambiguously revealed that six independent tweezers molecules of **1** engaged each other to provide the macrocycle (**1**)₆ of *S*₆ symmetry (Fig. 2a, Supplementary Figs. 19–20). The hexagonal assembly (**1**)₆ is ca. 22 Å in width and ca. 15 Å in height. The pyridine moiety of one molecule is intercalated by the two anthracene units of another molecule via a π - π interaction (ca. 3.4 Å for the C \cdots C distance, Fig. 2b). Twelve sets of global intermolecular NH \cdots OC hydrogen bonds are observed between one of the two carbonyl groups and the amide protons (ca. 2.2 Å, Fig. 2c). The non-covalent interaction (NCI) plot³⁰ also supported the presence of these interactions (Fig. 2d). As a consequence of intermolecular hydrogen bonding, the direction of bound **1** was regulated at ca. 90° (Supplementary Fig. 21a), which is relatively smaller than the value of 120° for the ideal hexagonal shape. However, since the PDA linker and the anthracenes are orthogonal to each other, the six tweezers consecutively assemble in a zigzag pattern with 90° twisting, resulting in a chair-like cyclohexane conformation (Supplementary Fig. 21a). This assembling style may stabilize the hexameric structure, which is constructed by the cooperation of multiple noncovalent bonds. To avoid steric hindrance, both 3-(9-anthryl)phenyl moieties in **1** were twisted; their C(carbonyl)-N(amide)-C(phenyl)-C(phenyl) dihedral angles were -100.1° and +169.5° (Supplementary Fig. 21b). Although the formation of (**1**)₆ by a dual interaction system can be deemed “crystallization-driven self-assembly”^{31–38}, the resultant assembly based on the dual interaction system is completely different from any previous examples, even among PDA-based coordination macrocycles^{39,40}.

As shown in the crystal packing, (**1**)₆ exists as an entirely independent assembly and stacks in a multilayered fashion. A few intermolecular π - π interactions among each hexamer (**1**)₆ are found with disordered CH₂Cl₂ and *n*-hexane (Supplementary Figs. 22,23). Two sets of anthracene moieties in **1** are in different environments: one is located inside and the other is along the side of the assembly. Notably, (**1**)₆ can be considered a triple-layered macrocycle (Fig. 2e). In particular, the three parts in **1** described in Supplementary Fig. 24 correspond to 1st, 2nd, and 3rd layers. All of the layers roughly configurate macrocycle-like appearances. A multilayered molecule has been greatly attractive as a synthetic target^{10,41–44}, but to the best of our knowledge, a macrocycle self-assembled in a triple-layered fashion has not been reported thus far. In the fluorescence spectra, whereas **1** showed a weak emission ($\Phi_F = 0.08$) in a chloroform solution, (**1**)₆ showed a relatively intense emission ($\Phi_F = 0.21$) in the solid state owing to the suppression of thermal deactivation by the tight packing (Supplementary Fig. 25).

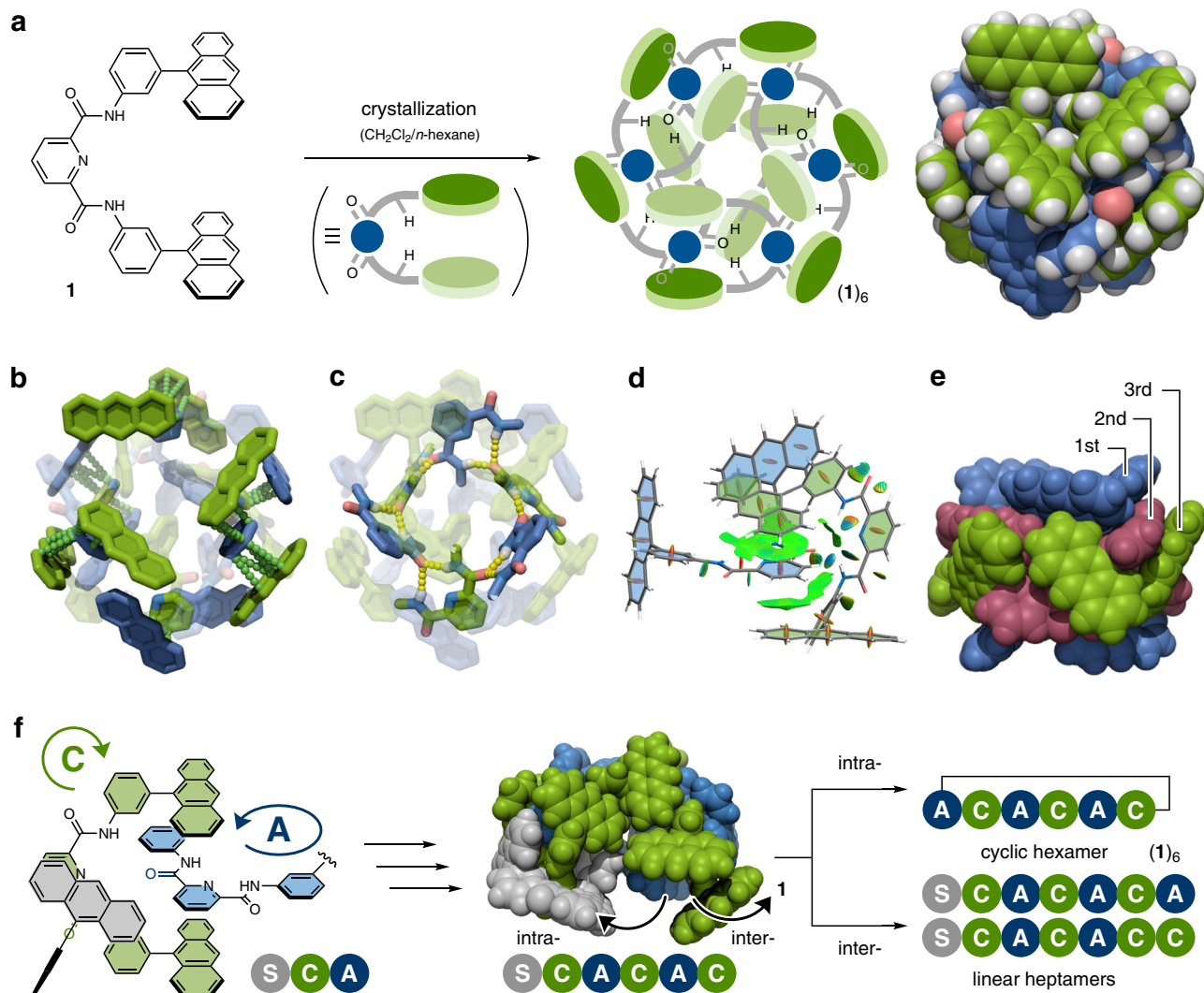


Fig. 2 | Formation of a self-complementary macrocycle. **a** Formation of self-complementary macrocycle $(\mathbf{1})_6$, and its X-ray crystal structure. Highlighted interactions in $(\mathbf{1})_6$: **b** π - π interactions (green dotted line) and **c** hydrogen bonding (yellow dotted line). **d** NCI plot calculated by the DFT method at the B3LYP-D3/6-31G(d,p) level. A single unit of the head-to-tail complex was extracted for clarity

(light green isosurface: π - π interaction; light blue isosurface: hydrogen bonding). **e** Representation of the triple-layered fashion of $(\mathbf{1})_6$ (blue: 1st-layer; red: 2nd-layer; green: 3rd-layer). **f** Schematic representation of the assembling process of $\mathbf{1}$ to form cyclic hexamer $(\mathbf{1})_6$ and linear heptamers.

Assembling process of the cyclic hexamer

The assembling process of $\mathbf{1}$ is remarkable. To construct cyclic hexamer $(\mathbf{1})_6$, six sets of assembly processes are required. Tweezers $\mathbf{1}$ of C_{2v} symmetry has two sets of hydrogen-donor and -acceptor units. To simplify the analysis, we defined the direction of bound $\mathbf{1}$ as “clockwise” (C) or “anticlockwise” (A) (Fig. 2f and Supplementary Figs. 26a, 27). In the 1st assembly with the initial tweezers (S), the binding site of captured $\mathbf{1}$ points clockwise (C) or anticlockwise (A) relative to the anthracene face of tweezers S, leading to the formation of SC and SA as achiral compounds (Fig. 2f and Supplementary Fig. 26b). For the 2nd assembly, the orientation of bound $\mathbf{1}$ was determined by looking from the top of the anthracene panel, with the hydrogen-bonded carbonyl at the bottom (Fig. 2f and Supplementary Fig. 26c). According to this rule, 32 kinds of diastereomeric linear heptamers (except for their enantiomers) are statistically formed after six sets of assemblies (Supplementary Fig. 26a). For instance, when all assembly processes occur in the “C” direction, the helical heptamer SCCCCC is provided (Supplementary Fig. 28). In the case of cyclic $(\mathbf{1})_6$, binding processes alternate from side to side, and the intramolecular sixth binding of SCACAC must occur between the sixth and initial tweezers S for ACACAC formation (Fig. 2f). On the other hand, the intermolecular

binding of SCACAC affords linear heptamer SCACACA or SCACACC (Fig. 2f).

Selective formation and thermal stability of the macrocycle

In the powder X-ray diffraction (PXRD) analysis of $(\mathbf{1})_6$, the diffraction peaks are well-consistent with those of the simulated pattern (Fig. 3a (upper left), and Supplementary Fig. 30). The well-matched PXRD pattern implies that the crystalline powders have only structure consists of cyclic hexamer $(\mathbf{1})_6$; no other structures like dimers nor linear oligomers. Due to the zigzag assembly, tweezers $\mathbf{1}$ cannot access the formation of odd-number cyclic oligomers (e.g., pentamer and heptamer). Steric hindrance and lack of structural rigidity might prevent the formation of tetramer and octamer, which are even-number cyclic oligomers (Supplementary Fig. 29). Furthermore, with the contribution of the crystal packing force, tweezers $\mathbf{1}$ exclusively forms the discrete cyclic hexamer $(\mathbf{1})_6$ in the solid state from at least 32 kinds of linear oligomers. Cyclic hexamer $(\mathbf{1})_6$ is relatively stable in the solid state. Although crystalline powders of $(\mathbf{1})_6$ were ground in a mortar for 3 min, PXRD diffraction peaks derived from $(\mathbf{1})_6$ were obviously found in the broad diffraction peak (Fig. 3a (lower left) and Supplementary Fig. 30). This result clearly revealed that the macrocyclic periodic

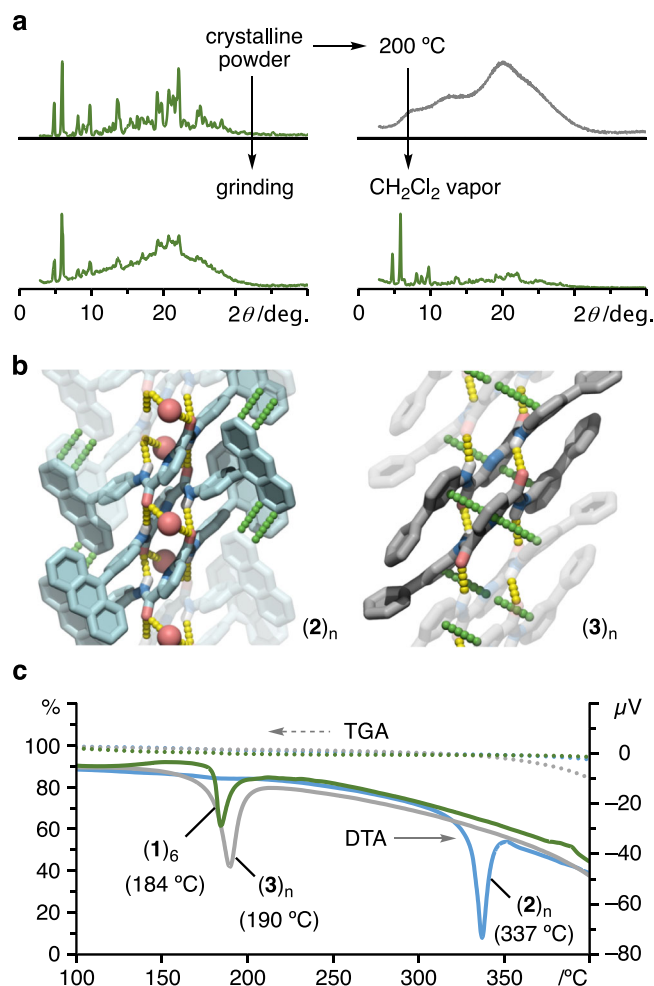


Fig. 3 | Structures and physical properties in the solid state. **a** PXRD patterns of the crystalline powders ($\mathbf{1}_6$), after grinding, and the bulk amorphous powders after heating at 200 °C and then exposure to CH_2Cl_2 vapor (intensities are shown as arbitrary units). **b** Packing structures of $\mathbf{2}$ and $\mathbf{3}$ in the single crystals. Yellow and green dotted lines indicate hydrogen bonding and π - π interactions, respectively. Red balls in the $(\mathbf{2})_n$ network are oxygen atoms of water molecules. **c** TG-DTA curves of $(\mathbf{1})_6$, $(\mathbf{2})_n$, and $(\mathbf{3})_n$ from 100 to 400 °C (dotted line: TGA curve, solid line: DTA curve).

structure remained in a large part of the structure while the other part becoming amorphous under mechanical stimulus. In contrast, cyclic hexamer ($\mathbf{1}_6$) disassembled into an amorphous state once the crystalline powders melted at 200 °C. As shown in Fig. 3a (upper right) and Supplementary Fig. 31, all PXRD diffraction peaks disappeared, and diffraction of a broad nature indicating an amorphous state was observed. Interestingly, when the bulk amorphous powders of $\mathbf{1}$ were exposed to CH_2Cl_2 vapor for 2 h, the hexameric structure of $\mathbf{1}$ was regenerated, as confirmed by the PXRD analysis. All diffraction peaks are perfectly consistent with those of $(\mathbf{1})_6$ (Fig. 3a (lower right) and Supplementary Fig. 31). The hexamer ($\mathbf{1}_6$) was exclusively formed even in the presence of polyaromatic compounds (e.g., anthracene and pyrene) as competitors. Attenuated total reflection Fourier transform infrared (ATR-FTIR) spectroscopy showed that $(\mathbf{1})_6$ exhibited two characteristic absorption bands due to amide C=O stretching at 1683 and 1656 cm^{-1} , whereas amorphous $\mathbf{1}$ displayed a broad absorption at approximately 1685 cm^{-1} due to various conformations and associations (Supplementary Fig. 32).

In sharp contrast, both $\mathbf{2}$ and $\mathbf{3}$, which have 4-(9-anthryl)phenyl and 3-biphenyl groups (Supplementary Figs. 7–16), respectively, as analogs of $\mathbf{1}$, displayed columnar packing structures $(\mathbf{2})_n$ and $(\mathbf{3})_n$ through intermolecular 1D hydrogen bonds and π -interactions (Fig. 3b

and Supplementary Figs. 33–36). Interestingly, the *m*-phenylene moieties of $\mathbf{3}$ inverted to form a linear structure rather than the tweezers form (Supplementary Fig. 35). As a consequence of these control experiments, we presumed that the 3-(9-anthryl)phenyl moieties play an important role in constructing discrete assemblies. The thermal stability of each assembly was evaluated by thermogravimetry-differential thermal analysis (TG-DTA) measurements over a range of 30 to 600 °C (Fig. 3c and Supplementary Fig. 37). The crystalline powders of $(\mathbf{1})_6$ displayed a single endothermic peak at 184 °C, which was assigned to the melting point. On the other hand, although $\mathbf{2}$ is a constitutional isomer of $\mathbf{1}$, $(\mathbf{2})_n$ showed an endothermic peak at 337 °C, which is dramatically higher than that of $(\mathbf{1})_6$. The observed high melting point arose from the robust intermolecular packing of $\mathbf{2}$, to which infinite hydrogen bonds and complementary CH- π interactions among the 4 sets of anthracenes contributed (Supplementary Fig. 34). The crystal of $(\mathbf{3})_n$ with a 1D hydrogen network exhibited an endothermic peak at 190 °C, the thermal stability of which was comparable to that of $(\mathbf{1})_6$ (Fig. 3c).

Hierarchical assembly of the macrocycle

Finally, we successfully constructed a further assembly based on cyclic hexamer ($\mathbf{1}_6$). When crystals of $\mathbf{1}$ were grown from $\text{CH}_2\text{Cl}_2/n$ -hexane in the presence of excess trifluoroacetic acid (TFA), trigonal-shaped pale-yellow crystals were obtained. According to X-ray analysis, surprisingly, cyclic hexamer ($\mathbf{1}_6$) constructed a spherical assembly $[(\mathbf{1})_6]_{18}$ (Fig. 4a and Supplementary Fig. 38). The spherical $[(\mathbf{1})_6]_{18}$ resulted in an assembly of 18 sets of $(\mathbf{1})_6$, which had a total of 108 molecules of $\mathbf{1}$ and was ca. 70 Å in diameter with a molecular weight of ca. 70 kDa (Fig. 4b and Supplementary Fig. 39a). The very large but relatively closed cavity within $[(\mathbf{1})_6]_{18}$ was calculated to be -10000 \AA^3 by the MoloVol program (Fig. 4c and Supplementary Fig. 39b)⁴⁵. Since cyclic hexamer ($\mathbf{1}_6$) forms in a biconcave-lens fashion, $(\mathbf{1})_6$ can interact with four other $(\mathbf{1})_6$ molecules between the side and concave area in a cross shape through π - π interactions, leading to the formation of a square assembly (Fig. 4d). The distances between the centroids of each side are 24.5 and 25.1 Å. Nearby square assemblies share one $(\mathbf{1})_6$ as a vertex with a 90° dihedral angle; consequently, $[(\mathbf{1})_6]_{18}$ forms a nearly complete cuboctahedron geometry. Notably, these phenomena from $\mathbf{1}$ towards $[(\mathbf{1})_6]_{18}$ via $(\mathbf{1})_6$ can be considered hierarchical assembly^{46,47}, which is reminiscent of the construction process of virus (e.g., HIV-1) capsids in nature^{2,4}. Two molecules of TFA as an additive were found at the diagonal position of $(\mathbf{1})_6$ with hydrogen bonds and halogen- π interactions⁴⁸ among hexamers, which may be induced to form a trigonal packing structure (Supplementary Fig. 40). The emission of $(\mathbf{1})_6$ was significantly quenched, probably due to charge-transfer between anthracene and electron deficient pyridyl-TFA complex⁴⁹. Furthermore, all assemblies $[(\mathbf{1})_6]_{18}$ independently existed and were separated by the rhombohedral grid $[(\mathbf{1})_6]_n$, which was also formed by $(\mathbf{1})_6$ in the crystal (Fig. 4e and Supplementary Figs. 41–42). The approximately 90 Å side of the unit grid is capable of encapsulating the $[(\mathbf{1})_6]_{18}$ assembly (Fig. 4f). All vertexes of cuboctahedron $[(\mathbf{1})_6]_{18}$ showed π - π interactions with grid sides and neighboring $[(\mathbf{1})_6]_{18}$ (Supplementary Fig. 43), which may contribute to stabilizing the giant assembly $[(\mathbf{1})_6]_{18}$.

Discussion

We have successfully synthesized a crystalline-driven self-complementary macrocycle reminiscent of Kekulé's monkey model based on consecutive host-guest complexations of molecular tweezers. The dual interaction system consisting of intermolecular π - π interactions and hydrogen bonds in concert provides exclusive formation of a cyclic hexamer in a triple-layered fashion from at least 32 types of linear isomers. The discrete and tight packing of the hexamer was well reflected in its fluorescent property and thermal stability. Furthermore, the cyclic hexamers transformed into both a giant spherical cuboctahedron composed of 108 molecular tweezers and

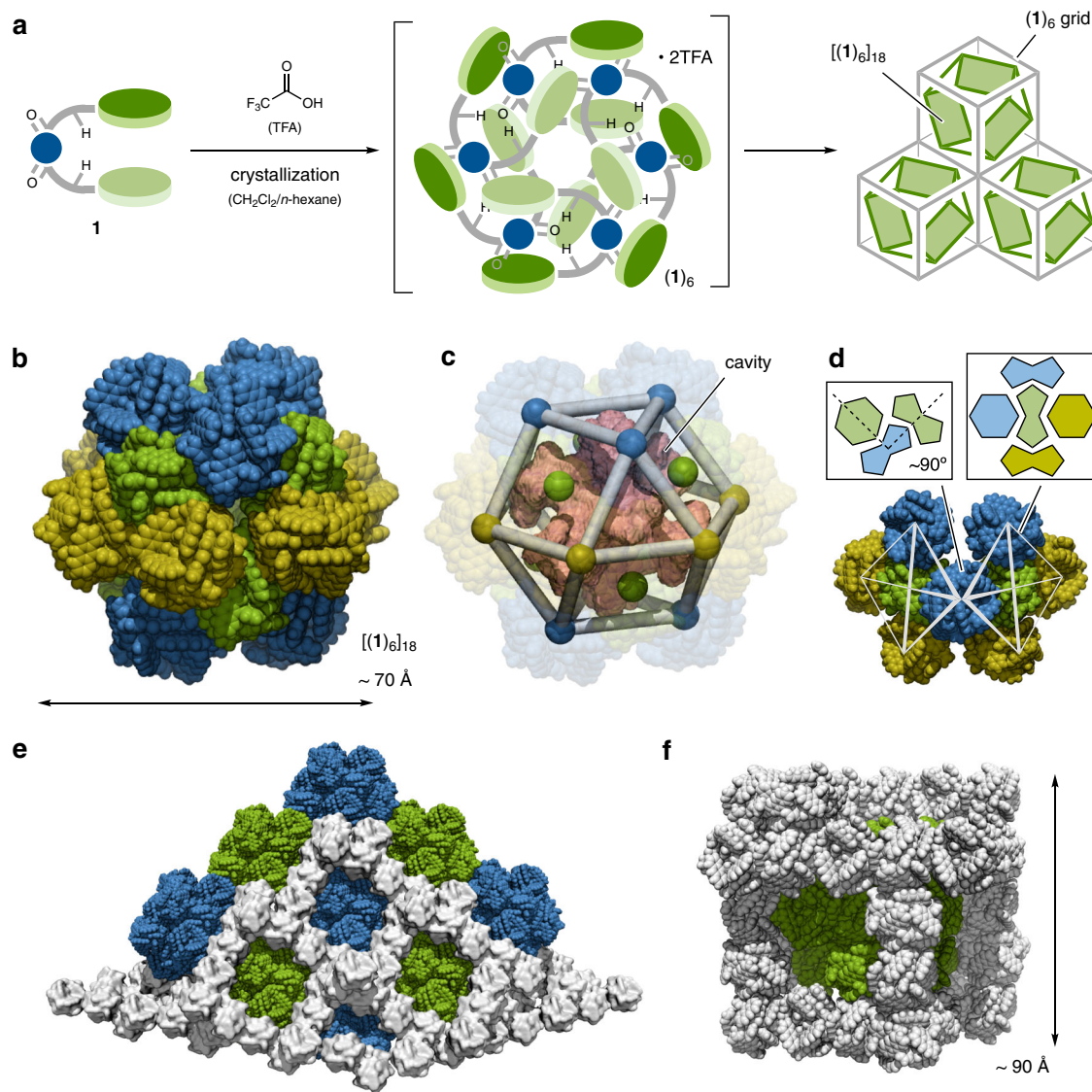


Fig. 4 | Hierarchical assembly based on $(\mathbf{1})_6$ in the solid state. **a** Formation of $[(\mathbf{1})_6]_{18}$ and $(\mathbf{1})_6$ grids by crystallization in the presence of TFA. **b, c** Extracted and schematic structures of $[(\mathbf{1})_6]_{18}$ with a cavity (pink color). To estimate the cavity, the relatively large holes on each surface of the cuboctahedron were obstructed by pseudoatoms with a 2.6 Å diameter. **d** Schematic representation of the assembly and

intermolecular interactions of each hexamer $(\mathbf{1})_6$. **e** Entire packing representation of trigonal crystal $(\mathbf{1})_6$. All assemblies $[(\mathbf{1})_6]_{18}$ are encapsulated within the $(\mathbf{1})_6$ grids in the crystal. Green and blue colors indicate $[(\mathbf{1})_6]_{18}$, and white color indicates $(\mathbf{1})_6$ grids. Some grid hexamers $(\mathbf{1})_6$ are omitted and displayed in surface representation for clarity. **f** Extracted set of $[(\mathbf{1})_6]_{18}$ (green color) and $(\mathbf{1})_6$ (white color) grids.

rhombohedral grid assemblies upon the simple addition of TFA as a result of hierarchical assembly. Although self-complementary assemblies have been well studied using various types of molecules and intermolecular interactions, we show a self-complementary assembly based on the host-guest system. The present strategy involving two types of effective intermolecular interactions might not only be one of chemical tools for constructing metal-free assemblies, but also a way for assembling anthracenes in a circle, such as a light-harvesting antenna protein complex⁵⁰.

Methods

General

All reagents and solvents were purchased from commercial sources and used as received. NMR spectra were recorded using a JEOL 500 MHz JNM-ECX500 spectrometer, a 500 MHz JNM-ECZ500 spectrometer, and a 400 MHz JNM-ECA400 spectrometer. Chemical shifts for ^1H , ^{13}C are reported in ppm on the δ scale; ^1H and ^{13}C signals were referenced to the residual solvent peak. Electrospray ionization time-of-flight (ESI-TOF) and high-resolution electrospray ionization mass

spectrometry (HRMS-ESI) were performed on a Bruker micrOTOF II mass Spectrometer. Attenuated Total Reflection Fourier transform infrared (ATR-FTIR) spectra were measured by a JASCO FT/IR 4100 and a Shimadzu IRSpirit. Elemental analyses were performed on a Perkin-Elmer 2400 instrument. Single crystal X-ray crystallography was carried out with a Rigaku XtaLAB Synergy R/DW HyPix diffractometer with multi-layer mirror monochromated $\text{Cu K}\alpha$ radiation ($\lambda = 1.54184 \text{ \AA}$) and processed on a CrysAlisPro 1.171 (Rigaku Oxford Diffraction, 2018). The structure was solved by direct methods using SHELXT-2014⁵¹ then refined and extended with SHELXL-2016⁵² using the OLex2.v1.2⁵³ graphical user interfaces. Powder X-ray diffraction data were collected for samples on Si plate on a Rigaku Miniflex 600 instruments in house using reflection mode (Cu X-ray source with D/tex Ultra2 detector, 2 theta range: 3–50°, scan step: 0.01°). All PXRD samples were measured without pre-grinding. Thermal analysis was carried out with a Shimadzu DTG-60 instrument. UV-visible absorption spectroscopy was performed using a JASCO V-650 UV-Vis-NIR spectrophotometer. Samples were analyzed using a quartz cuvette with optical path lengths of 10 mm. Fluorescence spectroscopy was performed using a JASCO

FP-8500 spectrofluorometer. Samples were analyzed at room temperature using quartz cuvettes with optical path lengths of 2.0 mm and 10 mm. Absolute fluorescence quantum yields were recorded on a Hamamatsu Quantaurus-QY C11347-01 with an integration sphere. All DFT calculations were performed by using Gaussian 16 program suite⁵⁴. Molecular mechanics calculation was conducted by CONFLEX program (version 8, CONFLEX Corp., Japan)^{55,56} and Material Studio program (version 5.5.3, BIOVIA, USA). The cavity volume was calculated by MoloVol with 2.6 Å pseudoatoms (grid resolution: 0.5 Å).

Synthesis of 1–3

2,6-Pyridinedicarboxylic acid (**A**; 3.34 g, 20.0 mmol) and dry-CH₂Cl₂ (20 mL) were added to a two-necked 100 mL flask under N₂ atmosphere. Oxalyl dichloride (7.70 g, 5.2 mL, 60.6 mmol) and dry-DMF (10 μL) were sequentially added to the flask at room temperature. The resultant mixture was stirred for 24 h at room temperature, and then the solvent was evaporated under reduced pressure. The obtained solid was washed with *n*-hexane to give 2,6-pyridinedicarbonyl dichloride (**B**) as a white solid (3.59 g, 17.6 mmol, 88%). **B** (0.416 g, 2.04 mmol) was dissolved in dry-CH₂Cl₂ (80 mL) and then transferred into a 100 mL dropping funnel under N₂. The solution was added dropwise to a solution of 9-(3-aminophenyl)anthracene (1.08 g, 4.01 mmol), triethylamine (2.0 mL), and dry-CH₂Cl₂ (8.0 mL) in a 300 mL two-necked flask over 3.5 h. The solution was stirred for 24 h at room temperature, and then the solvent was evaporated under reduced pressure. The crude mixture was dissolved in CHCl₃ and then poured into water (100 mL). The organic phase was separated, and the aqueous phase was extracted with CHCl₃ (50 mL×2). The combined organic extract was dried over Na₂SO₄, filtrated, and concentrated under reduced pressure. The obtained solid was washed with *n*-hexane to give **1** as a pale yellow solid (1.24 g, 91%). Under the same procedure, molecular tweezers **2** (81% yield) and **3** (99% yield) were prepared from 9-(4-aminophenyl)anthracene and 3-aminobiphenyl, respectively. Both single crystals of **2** and **3** were obtained from CH₂Cl₂/*n*-hexane at room temperature.

For 1

¹H NMR (500 MHz, CDCl₃, 293 K, 20 mM) δ 7.05 (d, *J* = 7.4 Hz, 2H), 7.15 (t, *J* = 7.4 Hz, 4H), 7.28 (t, *J* = 8.0 Hz, 1H), 7.32 (t, *J* = 7.4 Hz, 2H), 7.40 (t, *J* = 7.4 Hz, 2H), 7.43–7.48 (m, 6H), 7.69 (d, *J* = 7.4 Hz, 2H), 7.86 (d, *J* = 8.0 Hz, 2H), 7.89 (d, *J* = 8.6 Hz, 4H), 8.29 (s, 2H), 9.10 (s, 2H). ¹³C NMR (125 MHz, CDCl₃, 293 K, 20 mM) δ 119.6 (CH), 122.5 (CH), 124.9 (CH), 125.2 (CH), 125.5 (CH), 126.4 (CH), 126.7 (CH), 127.6 (CH), 128.4 (CH), 129.2 (CH), 129.8 (C_q), 131.2 (C_q), 135.9 (C_q), 137.3 (C_q), 137.9 (CH), 139.4 (C_q), 147.5 (C_q), 161.2 (C = O). HR MS (ESI-TOF, acetone): *m/z*: [M + Na]⁺ Calcd for C₄₇H₃₁N₃O₂Na, 692.2308; found 692.2327. FT-IR (amorphous, ATR, cm⁻¹): 3321, 3053, 1685, 1605, 1583, 1531, 1488, 1431, 1403, 1359, 1306, 1164, 1141, 1074, 1013, 1000, 881, 841.

For 2

¹H NMR (500 MHz, CDCl₃, 293 K, 10 mM) δ 7.37 (t, *J* = 7.5 Hz, 4H), 7.47 (t, *J* = 7.5 Hz, 4H), 7.54 (d, *J* = 8.0 Hz, 4H), 7.73 (d, *J* = 8.6 Hz, 4H), 8.01–8.10 (m, 8H), 8.27 (t, *J* = 8.0 Hz, 1H), 8.52 (s, 2H), 8.64 (d, *J* = 8.0 Hz, 2H), 9.75 (s, 2H). ¹³C NMR (125 MHz, CDCl₃, 293 K, 10 mM) δ 120.3 (CH), 125.3 (CH), 125.6 (CH), 126.1 (CH), 126.8 (CH), 126.9 (CH), 128.6 (CH), 130.4 (C_q), 131.5 (C_q), 132.4 (CH), 135.7 (C_q), 136.2 (C_q), 136.6 (C_q), 140.1 (CH), 149.2 (C_q), 161.4 (C = O). Note: Due to the low solubility of **2** in CDCl₃, the NMR spectra were measured at 10 mM. HR MS (ESI-TOF, acetone): *m/z*: [M + Na]⁺ calcd for C₄₇H₃₁N₃O₂Na, 692.2308; found 692.2315. Elemental analysis: Calcd for C₄₇H₃₁N₃O₂·(H₂O)_{1.3}·(CHCl₃)_{0.7}: C, 73.76; H, 4.45; N, 5.41. Found: C, 73.76; H, 4.20; N, 5.44.

For 3

¹H NMR (500 MHz, CDCl₃, 293 K, 20 mM) δ 7.36 (t, *J* = 7.2 Hz, 2H), 7.40–7.44 (m, 6H), 7.46 (t, *J* = 7.8 Hz, 2H), 7.60 (d, *J* = 7.2 Hz, 4H), 7.71 (d,

J = 7.8 Hz, 2H), 8.01 (s, 2H), 8.10 (t, *J* = 7.7 Hz, 1H), 8.48 (d, *J* = 7.7 Hz, 2H), 9.61 (s, 2H). ¹³C NMR (125 MHz, CDCl₃, 293 K, 20 mM) δ 119.3 (CH), 119.4 (CH), 124.0 (CH), 125.8 (CH), 127.3 (CH), 127.8 (CH), 129.0 (CH), 129.7 (CH), 137.6 (C_q), 139.7 (CH), 140.6 (C_q), 142.5 (C_q), 149.1 (C_q), 161.5 (C = O). HR MS (ESI-TOF, acetone): *m/z*: [M + Na]⁺ calcd for C₃₁H₂₃N₃O₂Na, 492.1688; found 492.1676. Elemental analysis: Calcd for C₃₁H₂₃N₃O₂·(H₂O)_{0.2}: C, 78.69; H, 4.99; N, 8.88. Found: C, 78.73; H, 4.91; N, 8.70.

Formation of self-complementary macrocycle (1)₆

Recrystallization of **1** from CH₂Cl₂/*n*-hexane (2:1) at room temperature for 1 day gave (1)₆ as a pale-yellow crystal. The formation of (1)₆ was confirmed by NMR and both single crystal and powder X-ray analyses.

¹³C NMR (100 MHz, solid, 293 K) δ 163.0, 146.3, 143.0–114.5. FT-IR (ATR, cm⁻¹): 3282, 3047, 1681, 1658, 1605, 1532, 1488, 1443, 1403, 1359, 1307, 1221, 1165, 1141, 1077, 1013, 1002, 953, 882, 841. Elemental analysis: Calcd for (C₄₇H₃₁N₃O₂)₆·(CH₂Cl₂)_{3.3}·(C₆H₁₄)_{0.3}: C, 79.73; H, 4.59; N, 5.83. Found: C, 79.68; H, 4.59; N, 5.85.

Formation of hierarchical assemblies based on (1)₆

Recrystallization of **1** from CH₂Cl₂/*n*-hexane (2:1) in the presence of trifluoroacetic acid (excess) at room temperature for 1 day gave (1)₆·(TFA)₂ as a pale-yellow crystal. The formation of (1)₆·(TFA)₂ was confirmed by single crystal X-ray analysis.

FT-IR (ATR, cm⁻¹): 3285, 3049, 2855, 2701, 2541, 1785, 1653, 1607, 1558, 1534, 1405, 1358, 1308, 1212, 1159, 1077, 1014, 1001, 884, 843, 790, 734, 702, 683, 595, 585, 554, 533, 425, 420. Elemental analysis: Calcd for (C₄₇H₃₁N₃O₂)₆·(CF₃COOH)₂·(CH₂Cl₂)_{3.5}·(C₆H₁₂)_{0.2}: C, 76.55; H, 4.37; N, 5.53. Found: C, 76.55; H, 4.20; N, 5.51.

Data availability

The authors declare that the data supporting the findings of this study are available within the Supplementary Information files and from the corresponding author upon request. CCDC 2158897, 2158909, 2158891, and 2158899 contain the supplementary crystallographic data for the structure reported in this article. The data can be obtained free of charge from The Cambridge Crystallographic Data Centre (CCDC) via www.ccdc.cam.ac.uk/data_request/cif.

References

1. Rebek, J. Jr Assembly and encapsulation with self-complementary molecules. *Chem. Soc. Rev.* **25**, 255–264 (1996).
2. Perlmutter, J. D. & Hagan, M. F. Mechanisms of virus assembly. *Annu. Rev. Phys. Chem.* **66**, 217–239 (2015).
3. Gres, A. T. et al. X-ray crystal structures of native HIV-1 capsid protein reveal conformational variability. *Science* **349**, 99–103 (2015).
4. Zhao, G. et al. Mature HIV-1 capsid structure by cryo-electron microscopy and all-atom molecular dynamics. *Nature* **497**, 643–646 (2013).
5. Conn, M. M. & Rebek, J. Jr Self-assembling capsules. *Chem. Rev.* **97**, 1647–1668 (1997).
6. Hof, F., Craig, S. L., Nuckolls, C. & Rebek, J. Jr Molecular encapsulation. *Angew. Chem. Int. Ed.* **41**, 1488–1508 (2002).
7. Adriaenssens, L. & Ballester, P. Hydrogen bonded supramolecular capsules with functionalized interiors: The controlled orientation of included guests. *Chem. Soc. Rev.* **42**, 3261–3277 (2013).
8. Luo, Q., Hou, C., Bai, Y., Wang, R. & Liu, J. Protein assembly: Versatile approaches to construct highly ordered nanostructures. *Chem. Rev.* **116**, 13571–13632 (2016).
9. Hiraoka, S., Nakamura, T., Shiro, M. & Shionoya, M. In-water truly monodisperse aggregation of gear-shaped amphiphiles based on hydrophobic surface engineering. *J. Am. Chem. Soc.* **132**, 13223–13225 (2010).

- Kim, H.-J. et al. Self-dissociating tubules from helical stacking of noncovalent macrocycles. *Angew. Chem. Int. Ed.* **49**, 8471–8475 (2010).
- Li, G.-L. et al. Constructing π -stacked supramolecular cage based hierarchical self-Assemblies via π - π stacking and hydrogen bonding. *J. Am. Chem. Soc.* **143**, 10920–10929 (2021).
- Tang, M. et al. Molecular-strain engineering of double-walled tetrahedra. *Chem* **7**, 2160–2174 (2021).
- Tsuda, A., Nakamura, T., Sakamoto, S., Yamaguchi, K. & Osuka, A. A self-assembled porphyrin box from meso-meso-linked bis[5-*p*-pyridyl-15-(3,5-di-octyloxyphenyl)porphyrinato zinc(II)]. *Angew. Chem. Int. Ed.* **41**, 2817–2821 (2002).
- Takahashi, R. & Kobuke, Y. Hexameric macroring of gable-porphyrins as a light-harvesting antenna mimic. *J. Am. Chem. Soc.* **125**, 2372–2373 (2003).
- Houk, K. N., Leach, A. G., Kim, S. P. & Zhang, X. Binding affinities of host-guest, protein-ligand, and protein-transition-state complexes. *Angew. Chem. Int. Ed.* **42**, 4872–4897 (2003).
- Bier, D. et al. Molecular tweezers modulate 14-3-3 protein-protein interactions. *Nat. Chem.* **5**, 234–239 (2013).
- Rotzler, J. & Mayor, M. Molecular daisy chains. *Chem. Soc. Rev.* **42**, 44–62 (2013).
- Yang, X., Wang, R., Kermagoret, A. & Bardelang, D. Oligomeric cucurbituril complexes: From peculiar assemblies to emerging applications. *Angew. Chem. Int. Ed.* **59**, 21280–21292 (2020).
- Leblond, J. & Petitjean, A. Molecular tweezers: Concepts and applications. *ChemPhysChem* **12**, 1043–1051 (2011).
- Hardouin-Lerouge, M., Hudhomme, P. & Sallé, M. Molecular clips and tweezers hosting neutral guests. *Chem. Soc. Rev.* **40**, 30–43 (2011).
- Kumar, P. & Gupta, R. The wonderful world of pyridine-2,6-dicarboxamide based scaffolds. *Dalton Trans.* **45**, 18769–18783 (2016).
- Zhan, C., Léger, J. M. & Huc, I. Cross-hybridization of pyridinedicarboxamide helical strands and their *N*-oxides. *Angew. Chem. Int. Ed.* **45**, 4625–4628 (2006).
- Haino, T., Fujii, T. & Fukazawa, Y. Guest binding and new self-assembly of bisporphyrins. *J. Org. Chem.* **71**, 2572–2580 (2006).
- Kim, S. K. et al. Self-association and nitroaromatic-induced deaggregation of pyrene substituted pyridine amides. *J. Am. Chem. Soc.* **136**, 495–505 (2014).
- Hirao, T., Hisano, N., Akine, S., Kihara, S.-I. & Haino, T. Ring-chain competition in supramolecular polymerization directed by molecular recognition of the bisporphyrin cleft. *Macromolecules* **52**, 6160–6168 (2019).
- Frischmann, P. D., Guieu, S., Tabeshi, R. & MacLachlan, M. J. Columnar organization of head-to-tail self-assembled Pt₄ rings. *J. Am. Chem. Soc.* **132**, 7668–7675 (2010).
- Wu, R. T., Chi, X., Hirao, T., Lynch, V. M. & Sessler, J. L. Supramolecular properties of a monocarboxylic acid-functionalized “texas-sized” molecular box. *J. Am. Chem. Soc.* **140**, 6823–6831 (2018).
- Wilcox, D. H. Jr & Greenbaum, F. R. Kekulé’s benzene ring theory: A subject for lighthearted banter. *J. Chem. Educ.* **42**, 266–267 (1965).
- Han, Y., Tian, Y., Li, Z. & Wang, F. Donor-acceptor-type supramolecular polymers on the basis of preorganized molecular tweezers/guest complexation. *Chem. Soc. Rev.* **47**, 5165–5176 (2018).
- Johnson, E. R. et al. Revealing noncovalent interactions. *J. Am. Chem. Soc.* **132**, 6498–6506 (2010).
- Moulton, B. & Zaworotko, M. J. From molecules to crystal engineering: Supramolecular isomerism and polymorphism in network solids. *Chem. Rev.* **101**, 1629–1658 (2001).
- Qiu, H. et al. Branched micelles by living crystallization-driven block copolymer self-assembly under kinetic control. *J. Am. Chem. Soc.* **137**, 2375–2385 (2015).
- Teyssandier, J., Feyter, S., De & Mali, K. S. Host-guest chemistry in two-dimensional supramolecular networks. *Chem. Commun.* **52**, 11465–11487 (2016).
- Yamasaki, Y., Sekiya, R. & Haino, T. Hexameric assembly of 5,17-disubstituted calix[4]arene in the solid state. *CrystEngComm* **19**, 6744–6751 (2017).
- Zhou, Y., Jie, K., Zhao, R. & Huang, F. Supramolecular-macrocycle-based crystalline organic materials. *Adv. Mater.* **32**, 1904824 (2020).
- Guo, Q.-H. et al. A hierarchical nanoporous diamondoid superstructure. *Chem* **5**, 2353–2364 (2019).
- Isoda, K., Haga, H., Kamebuchi, H. & Tadokoro, M. Crystallization-induced planar chirality by asymmetric ferrocene-appended tetra-azanaphthacene. *Cryst. Growth Des.* **20**, 7081–7086 (2020).
- Somsri, S., Kuwamura, N., Kojima, T., Yoshinari, N. & Konno, T. Self-assembly of cyclic hexamers of γ -cyclodextrin in a metallosupramolecular framework with D-penicillamine. *Chem. Sci.* **11**, 9246–9253 (2020).
- Belli Dell’Amico, D. et al. Coordination properties towards palladium(II) of a tridentate dianionic ligand acting as a N- or a N,O-donor. *Inorg. Chim. Acta* **359**, 127–135 (2006).
- Wang, Q. Q., Day, V. W. & Bowman-James, K. Hexagonal molecular “palladawheel”. *Chem. Commun.* **49**, 8042–8044 (2013).
- Sun, Q.-F., Murase, T., Sato, S. & Fujita, M. A sphere-in-sphere complex by orthogonal self-assembly. *Angew. Chem. Int. Ed.* **50**, 10318–10321 (2011).
- Hashimoto, S., Iwamoto, T., Kurachi, D., Kayahara, E. & Yamago, S. Shortest double-walled carbon nanotubes composed of cycloparaphenylenes. *ChemPlusChem* **82**, 1015–1020 (2017).
- Tamura, Y., Takezawa, H. & Fujita, M. A Double-walled knotted cage for guest-adaptive molecular recognition. *J. Am. Chem. Soc.* **142**, 5504–5508 (2020).
- Cai, K. et al. Molecular Russian dolls. *Nat. Commun.* **9**, 5275 (2018).
- Maglic, J. B. & Lavendomme, R. MoloVol: an easy-to-use program to calculate various volumes and surface areas of chemical structures and identify cavities. *J. Appl. Cryst.* **55**, 1033–1044 (2022).
- Datta, S., Saha, M. L. & Stang, P. J. Hierarchical assemblies of supramolecular coordination complexes. *Acc. Chem. Res.* **51**, 2047–2063 (2018).
- Ronson, T. K. et al. Stellated polyhedral assembly of a topologically complicated Pd₄L₄ ‘Solomon cube’. *Nat. Chem.* **1**, 212–216 (2009).
- Saraogi, I., Vijay, V. G., Das, S., Sekar, K. & Guru Row, T. N. C-halogen... π interactions in proteins: A database study. *Cryst. Eng.* **6**, 69–77 (2003).
- Zhao, G.-J. & Han, K.-L. Ultrafast hydrogen bond strengthening of the photoexcited fluorenone in alcohols for facilitating the fluorescence quenching. *J. Phys. Chem. A* **111**, 9218–9223 (2007).
- Niwa, S. et al. Structure of the LH1-RC complex from *Thermochromatium tepidum* at 3.0 Å. *Nature* **508**, 228–232 (2014).
- Sheldrick, G. M. SHELXT - Integrated space-group and crystal-structure determination. *Acta Crystallogr. A* **71**, 3–8 (2015).
- Sheldrick, G. M. Crystal structure refinement with SHELXL. *Acta Crystallogr. C* **71**, 3–8 (2015).
- Dolomanov, O. V., Bourhis, L. J., Gildea, R. J., Howard, J. A. K. & Puschmann, H. OLEX2: a complete structure solution, refinement and analysis program. *J. Appl. Crystallogr.* **42**, 339–341 (2009).
- Gaussian 16, Revision C.01. Frisch, M. J. et al. Gaussian, Inc., Wallingford CT, USA (2016).
- Gotō, H. & Ōsawa, E. Corner flapping: a simple and fast algorithm for exhaustive generation of ring conformations. *J. Am. Chem. Soc.* **111**, 8950–8951 (1989).
- Gotō, H. & Ōsawa, E. An efficient algorithm for searching low-energy conformers of cyclic and acyclic molecules. *J. Chem. Soc., Perkin Trans.* **2**, 187–198 (1993).

Acknowledgements

This study was supported by JSPS Grant-in-Aid for Scientific Research (JP20H02721) for S.T., Grant-in-Aid for Research Activity Start-up (JP19K23623) for M.Y., Grant-in-Aid for Early-Career Scientists (JP20K15255) for M.Y., Yoshinori Ohsumi Fund for Fundamental Research for M.Y. We thank Tokyo Institute of Technology Open Facility Center for performing mass and thermal analyses. We appreciate Prof. Nobuharu Iwasawa (Tokyo Tech.) and Prof. Masaki Kawano (Tokyo Tech.) for X-ray analyses, Prof. Michito Yoshizawa (Tokyo Tech.) for the solid-state optical measurements, and Prof. Kei Goto (Tokyo Tech.), Prof. Kosuke Ono (Tokyo Tech.) and Dr. Yuya Tanaka (Tokyo Tech.) for the ATR-FTIR measurements. We also appreciate valuable discussions with Prof. Gaku Fukuhara (Tokyo Tech.) and Dr. Eiji Tsurumaki (Tokyo Tech.).

Author contributions

Y.S., M.Y., and S.T. designed the work, carried out research, and wrote the paper. H.O. contributed to X-ray crystallographic analysis. M.Y. and S.T. are the corresponding authors. All authors discussed the results and commented on the manuscript.

Competing interests

The authors declare no competing interests.

Additional information

Supplementary information The online version contains supplementary material available at <https://doi.org/10.1038/s41467-022-33357-y>.

Correspondence and requests for materials should be addressed to Masahiro Yamashina or Shinji Toyota.

Peer review information *Nature Communications* thanks the anonymous reviewer(s) for their contribution to the peer review of this work.

Reprints and permission information is available at <http://www.nature.com/reprints>

Publisher's note Springer Nature remains neutral with regard to jurisdictional claims in published maps and institutional affiliations.

Open Access This article is licensed under a Creative Commons Attribution 4.0 International License, which permits use, sharing, adaptation, distribution and reproduction in any medium or format, as long as you give appropriate credit to the original author(s) and the source, provide a link to the Creative Commons license, and indicate if changes were made. The images or other third party material in this article are included in the article's Creative Commons license, unless indicated otherwise in a credit line to the material. If material is not included in the article's Creative Commons license and your intended use is not permitted by statutory regulation or exceeds the permitted use, you will need to obtain permission directly from the copyright holder. To view a copy of this license, visit <http://creativecommons.org/licenses/by/4.0/>.

© The Author(s) 2022